Carbohydrate Polymers 86 (2011) 1118–1129

Contents lists available at ScienceDirect

Carbohydrate Polymers

journal homepage: www.elsevier.com/locate/carbpol

Folate-modified chitosan micelles with enhanced tumor targeting evaluated by near infrared imaging system

Hongyan Zhu[a,b], Fei Liu[a], Jing Guo[a], Jianpeng Xue[a], Zhiyu Qian[c], Yueqing Gu[a,*]

[a] Department of Biomedical Engineering, School of Life Science and Technology, China Pharmaceutical University, Nanjing 210009, China
[b] Department of Pharmacology, Medical College, Nantong University, Nantong 226001, China
[c] Department of Biomedical Engineering, School of Automation, Nanjing University of Aeronautics and Astronautics, Nanjing 210016, China

ARTICLE INFO

Article history:
Received 21 February 2011
Received in revised form 24 May 2011
Accepted 26 May 2011
Available online 6 June 2011

Keywords:
Chitosan
Micelles
Folate
Near infrared imaging
Bel-7402

ABSTRACT

Folate modified chitosan micelles were synthesized for cancer-specific targeting and drug delivery. Receptor-mediated uptake and drug delivery were characterized *in vitro* and in a small animal model of cancer after loading with hydrophobic fluorescent dyes as drug models. Hydrophilic succinic anhydride and hydrophobic octaldehyde were reacted with chitosan respectively to form amphipathic N-succinyl-N′-octyl chitosan (SO-chitosan). SO-chitosan was covalently modified with folate to form folate-modified N-succinyl-N′-octyl chitosan (folate-SO-chitosan). The folate-SO-chitosan micelles were obtained through self-assembling and maintained a stable core-shell structure with average diameter of about 136 nm up to 15 days. The prepared folate-SO-chitosan micelles displayed a good drug loading content (12.17%), entrapment efficiency (69.32%) and sustained release behavior for the model drug fluorescein. The *in vitro* cellular uptake and *in vivo* tumor targeting ability of the folate-SO-chitosan micelles were evaluated by fluorescence microscopy and near infrared imaging, respectively. *In vitro* and *in vivo* results demonstrated enhanced targeting behaviors in a folate receptor positive tumor model (Bel-7402), which suggests that the folate-SO-chitosan micelles are promising tumor targeting carriers for hydrophobic diagnostic agents as well as anti-tumor agents.

1. Introduction

Targeted nano-scaled drug delivery systems are the subject of intense as targeted carriers of therapeutics and/or diagnostics agents to diseased tissues, which enables improved systemic performance efficiency as well as reduced adverse effects. Chitosan, an abundant natural biopolymer, is a popular choice for basis of some nano-scaled drug delivery systems. Chitosan-based nanoparticles (Calvo, Remunan, Vila, & Alonso, 1997), microspheres (Rege, Shukla, & Block, 1999), hydrogels (Mi et al., 1999), films (Tomihata & Ikada, 1997), fibers (Hirano, Zhang, Nakagawa, & Miyata, 2000) and tablets (Rege, Garmise, & Block, 2003) have shown advantages such as high biocompatibility, bio-degradation, hydrophilicity, and low toxicity toward mammalian cells (Felt, Buri, & Gurny, 1998; Illum, 1998). Active hydroxyl and amine groups in the backbone of chitosan allow simple chemical modification to form a large variety of multifunctional structures including micelles. Chitosan-based micellar systems are known to possess great potential in biological applications by introducing hydrophobic and/or hydrophilic groups to the chitosan backbone. For example, the water-soluble micellar shell provides a steady interface between the insoluble core and the external circumference. This shell also enables micelle to maintain *in vivo* long circulation (Rösler, Vandermeulen, & Klok, 2001; Wei, Cheng, Zhang, & Zhuo, 2009). The hydrophobic core creates a friendly microenvironment for incorporated lipophilic drugs. For these reasons, micellar drug delivery systems have been widely studied as the delivery vehicles for genetic material (Hu, Zhao, & Yuan, 2006), peptides (Park et al., 2004) and anti-tumor drugs (Zhang, Ding, Yu, & Ping, 2007).

Of note, polymeric micelles exhibit the ability to accumulate at the solid tumor site by the so-called enhanced permeation and retention effect (Maeda, Bharate, & Daruwalla, 2009). Such passive targeting can increase the accumulation of the drugs or imaging agents in tumor site, however the spread of the agents in other tissues is still a concern and the tumor specificity by this mechanism is limited. In order to selectively deliver the micelles to tumor tissues, active targeting through tumor-specific antigen/antibody and ligand/receptor interaction has been widely investigated (Gan & Feng, 2010; Saad et al., 2008). Among these strategies, we chose to modify the surface of chitosan micelles with folic acid to deliver attached cargoes to folate receptor pos-

* Corresponding author. Tel.: +86 25 83271046; fax: +86 25 83271046.
E-mail address: guyueqingsubmission@hotmail.com (Y. Gu).

0144-8617/$ – see front matter © 2011 Elsevier Ltd. All rights reserved.
doi:10.1016/j.carbpol.2011.05.061

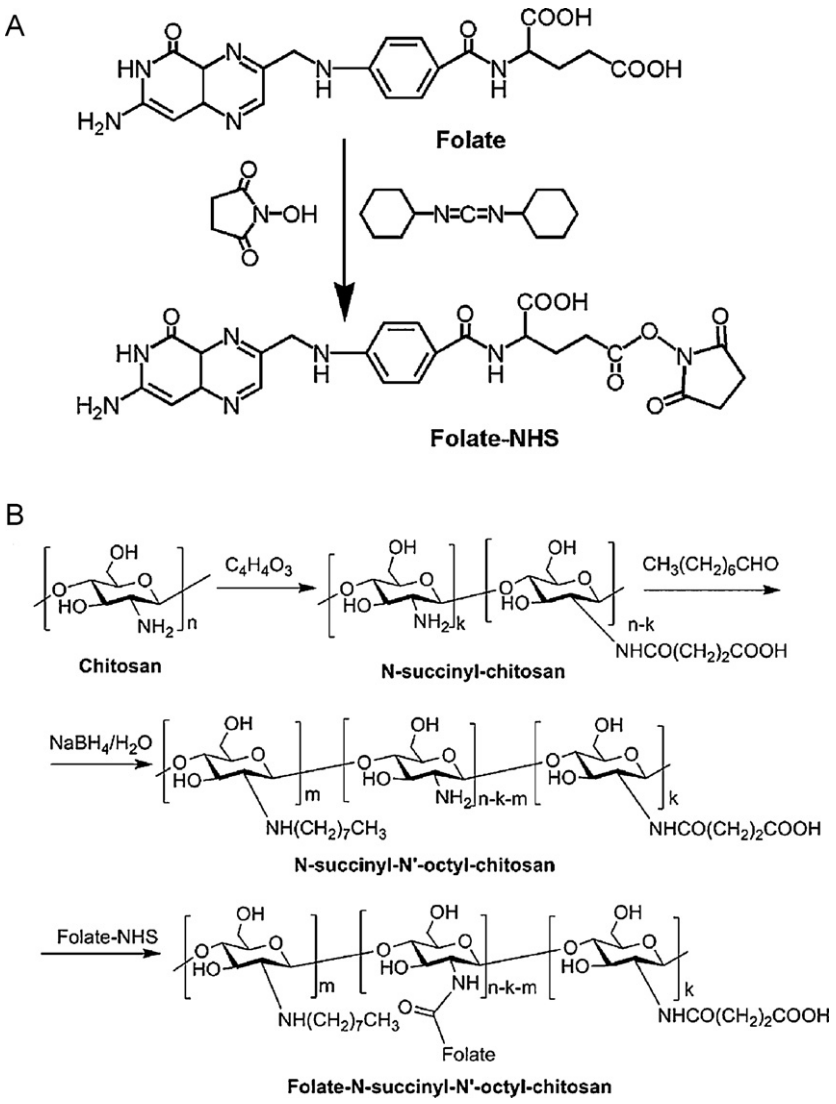

Fig. 1. Synthesis of folate-modified N-succinyl-N′-octyl chitosan: (A) activation of folate; (B) synthesis of N-succinyl-N′-octyl chitosan and folate-SO-chitosan.

itive cancer cells. Folate receptor is highly expressed in several human tumor cells including cancers of the ovary, breast, liver, kidney, uterus, testis, brain, colon and lung (Hilgenbrink & Low, 2005). Folate and folate conjugates can bind to the folate receptor with high affinity and enter cells by receptor-mediated endocytosis (Leamon & Low, 2001; Sabharanjak & Mayor, 2004). Since the folate receptor-mediated endocytosis was discovered, folate-based candidates have been widely used for targeted drug delivery, especially in the research field of molecular imaging (Corot et al., 2008; Kamaly, Kalber, Thanou, Bell, & Miller, 2009). However, no report has been found to conjugate folate to amphiphilic chitosan micelles for targeted delivery of anticancer drugs/diagonsitic agents.

Optical imaging provides a convenient way to study the *in vitro* cellular uptake and *in vivo* dynamic distribution of drugs in small animal subjects. In this study, we chose fluorescent dyes, fluorescein and ICG derivative, as two model drugs for *in vitro* celluar study and *in vivo* targeting evaluation, respectively. To the best of our knowledge, this is the first report of synthesis and evaluation of folate-modified amphiphilic chitosan micelles for *in vivo* tumor imaging and drug delivery.

2. Materials and methods

2.1. Materials

Chitosan was purchased from Aoxing Biotechnology Co. Ltd. (Zhejiang, China), with deacetylation degrees of 90% and average molecular weight (MW) of 10 kDa. Folic acid (folate, MW 441), N,N′-dicyclohexylcarbodiimide (DCC), N-hydroxysuccinimide (NHS) and methyl thiazolyl tetrazolium (MTT) were all purchased from Sigma–Aldrich (St. Louis, USA). Indocyanine Green (ICG) derivative (MW 689) was prepared in our laboratory. Fluorescein was purchased from Aladdin reagent (Shanghai, China). RPMI 1640 medium, folate-free RPMI 1640 medium, calf serum, penicillin, streptomycin, trypsin and ethylenediaminetetraacetic acid (EDTA) were all purchased from Invitrogen-Life Technologies (Carlsbad, CA, USA). The other chemical reagents used in the study were all commercially acquired from Shanghai Chemical Reagent Company (Shanghai, China) with analytical reagent grade.

Human hepatoma cell line (Bel-7402), human lung carcinoma cell line (A549) and human embryonic lung fibroblast cell line (HELF) were all purchased from American Type Culture Collection

(ATCC, Manassas, VA, USA). Athymic nude mice (nu/nu CD-1 male and female) were purchased from SLAC Laboratory Animal Co. Ltd. (Shanghai China).

2.2. Synthesis of folate-modified N-succinyl-N′-octyl-chitosan (folate-SO-chitosan)

2.2.1. Preparation of N-succinyl-N′-octyl-chitosan (SO-chitosan)

SO-chitosan was synthesized using a previously reported method (Xu et al., 2007). A schematic of the synthesis of SO-chitosan is depicted in Fig. 1. Briefly, chitosan (1 g) was reacted with 3 g succinic anhydride dissolved in 17 mL acetone solution, followed by constant stirring for 48 h at room temperature. After the reaction, the resultant mixture was precipitated with 5% (w/v) NaOH and then filtered. The precipitate (N-succiny-chitosan) was washed with alcohol for three times and then dried under vacuum at 60 °C overnight. Next, N-succinyl-chitosan (1 g) was further reacted with octaldehyde (1.02 g). After constant stirring for 4 h, 1.6 mL $NaBH_4$ solution (10 mg/mL) was dropwise added to the mixture and followed by continuous stirring for 12 h. The product solution (SO-chitosan) was neutralized with 5% (w/v) NaOH then purified by dialysis (molecular weight cut off (MWCO) 10000).

2.2.2. Preparation of folate-SO-chitosan

Folate-SO-chitosan was synthesized in two steps. Firstly, the γ-COOH group of folic acid (22 mg) was activated by DCC/NHS catalyst systems (molar ratio of folate:DCC:NHS = 1:1.2:2) in anhydrous dimethyl sulfoxide (DMSO, 2.5 mL) under the continuous stirring in the dark for 12 h at room temperature. Secondly, the activated folic acid was added dropwise into the above SO-chitosan solution with stable stirring for 12 h. The activated γ-COOH group of folic acid was then reacted with the free amine group on the surface of SO-chitosan to form folated-modified SO-chitosan. The product was purified by dialysis (MWCO 10000) against distilled water for further research.

2.3. Characterization of folate-SO-chitosan micelles

The UV–vis absorption spectra, fourier transform infrared (FTIR) spectra and ^{1}H nuclear magnetic resonance (^{1}H NMR) spectra of folate-SO-chitosan micelles were recorded by UV–vis spectrophotometer (JH 754PC, China), FTIR spectrometer (Nicolet ECO 2000, USA) and NMR spectrometer (Bruker AV-500 NMR Spectrometer, Germany), respectively.

The size distribution and morphology of non-drug loaded folate-SO-chitosan micelles were characterized by Mastersizer 2000 Laser Particle Size Analyzer (LPSA, Malvern, British) and transmission electron microscope (TEM, Philips FEI Tecnai G2 20s-TWIN, the Netherlands) with accelerated voltage of 200 kV, respectively.

2.4. Drug loading and in vitro drug release

Two hydrophobic model drugs, fluorescein and ICG derivative, with different hydrophobicities, were chosen in this study to investigate the drug loading and release properties of folate-SO-chitosan. Each model drug (5 mg) was firstly dissolved in 0.5 mL DMSO and then dropwise added to 5 mL PBS solution (containing 25 mg folate-SO-chitosan) respectively under magnetic stirring at room temperature. Then, the solutions were placed into a dialysis tube (MWCO 10000) against 2 L distilled water for 24 h. After dialysis, centrifugation (12,000 rpm × 10 min) was carried out to remove the deposition of unloaded model drugs. In order to determine the entrapment efficiency of folate-SO-chitosan for the two model drugs, the drug loaded micelle solutions were lyophilized, dissolved in DMSO, and analyzed by measuring the absorbances of the resultant solutions at the absorption peaks of the two model drugs, respectively. The entrapment efficiency and drug loading content were calculated according to the following equations: entrapment efficiency = (mass of drug loaded in micelles/mass of drug fed initially) × 100%; drug loading content = (mass of drug loaded in micelles/mass of drug loaded micelles) × 100%.

The release profiles of model drugs from folate-SO-chitosan micelles *in vitro* were tested by a dialysis method. Drug (fluorescein/ICG derivative) loaded folate-SO-chitosan solution was dialyzed (MWCO 10000) against phosphate buffered saline (PBS) in dark environment at 37 °C. The released model drug (fluorescein/ICG derivative) in the incubation buffer was collected and the aliquots taken from the dialysate were replaced with fresh PBS at predetermined time intervals to keep the volume constant during the assay. The concentration of the released model drugs was determined by UV–vis spectrophotometer.

2.5. Optical characterization of free and entrapped ICG derivative

Absorbance and fluorescence spectra of free and entrapped ICG derivative were measured by UV–vis spectrophotometer and S2000 spectrometer (Ocean Optics, USA), respectively. The photostability of free and entrapped ICG derivative was evaluated by measuring their relative fluorescence intensity under continuous exposure to the laser for 1 h, with 5 min interval for data acquisition.

2.6. In vitro cytotoxicity study

Bel-7402, A549 and HELF cells were cultured continuously at 37 °C in a humidified atmosphere containing 5% CO_2 in folate-free RPMI 1640 medium supplemented with 10% (v/v) calf serum, penicillin (100 U/mL) and streptomycin (100 μg/mL) in wells of 96-well plate. 200 μL RPMI 1640 medium containing SO-chitosan or folate-SO-chitosan with particular concentrations (0.0625, 0.125, 0.25, 0.5, 1, 2 mg/mL) was added into each well in a 96-well plate. After incubation for 48 h, the RPMI 1640 medium with polymers was replaced by 180 μL fresh RPMI 1640 medium and 20 μL MTT solution (5 mg/mL). After incubation for another 4 h, culture medium was removed and 200 μL DMSO was added into each well. The optical density (OD) was measured at 570 nm (determination wavelength) and 630 nm (background wavelength) with a Microplate Reader Model 550 (BIO-RAD, USA). Cell viability (%) = $(OD_{treated}/OD_{control}) \times 100\%$, where $OD_{treated}$ was obtained in the presence of SO-chitosan or folate-SO-chitosan and $OD_{control}$ was obtained in the absence of SO-chitosan or folate-SO-chitosan.

2.7. Determination of folate receptor expression level by reverse transcriptase-polymerase chain reaction (RT-PCR)

Total RNA was extracted from freshly isolated A549/Bel-7402 cells using RNeasy kit. Three micrograms of RNA from each cell was converted into cDNA with SuperScript™ III Reverse Transcriptase. Then 1 μL cDNA was used for PCR amplification using folate receptor-specific primers: the forward primer, 5′-ACACCAGCCAGGAAGCCCATA-3′, the reverse primer, 5′-GAGCAGCCACAGCAGCATTAG-3′. 5 μL products (563 bp) were used for 2% (w/v) agarose gel electrophoresis.

2.8. In vitro cellular uptake evaluated by fluorescence microscopy and flow cytometer

Bel-7402 and A549 cells were cultured in the 24-well plates for the cell internalization study of folate-SO-chitosan micelles. 0.5 mL fresh folate-free RPMI 1640 medium containing 100 μg fluorescein-loaded SO-chitosan or folate-SO-chitosan micelles was added into each well. After incubation for 6 h, the medium was removed and cells were washed with PBS solution three times.

Then, 0.5 mL PBS solution was added in each well. The fluorescent images of the cells were observed under excitation at 488 nm using the fluorescence microscopy (Olympus BX60, Japan).

To quantify the uptake of the SO-chitosan and folate-SO-chitosan micelles to the different tumor cells, a flow cytometer was used (Beckman Coulter, USA). 2 mL folate-free RPMI 1640 medium containing 400 μg fluorescein-loaded micelles was added into each well containing 10^6 Bel-7402 or A549 cells. Then, the culture medium was removed and the cells were incubated in 2 mL of PBS containing 10% (v/v) calf serum. After 6 h of incubation, the medium was removed and the cells were washed 3 times with 2 mL of PBS. The cells were detached by 0.25% (w/v) trypsin, resuspended in 500 μL of PBS and analyzed by the flow cytometer immediately.

For folate competition assay, Bel-7402 cells were firstly incubated in folate-free RPMI 1640 supplemented with 10% (v/v) calf serum for 24 h and then exposed to 1 mM free folic acid for 30 min before adding 2 mL medium containing fluorescein-loaded folate-SO-chitosan (400 μg). After that, cells were treated in the same way as described above.

2.9. In vivo tumor targeting ability of folate-SO-chitosan micelles evaluated by NIR imaging system

The athymic nude mice used in this study were 4–6 weeks old and weighed at about 18–22 g. Each mouse was anesthetized with isoflurane before being injected subcutaneously under left armpit with 0.1 mL sterile PBS containing 3×10^6 tumor cells (Bel-7402 cells or A549 cells). After the mean diameters of tumor mass reached 2–5 mm in volume, the mice were used for *in vivo* imaging studies. All animal experiments were carried out in compliance with the Animal Management Rules of the Ministry of Health of the People's Republic of China (document no. 55, 2001), the guidelines for the Care and Use of Laboratory Animals of China Pharmaceutical University and Principles of Laboratory Animal Care (NIH publication #85-23, revised in 1985).

Twenty-five athymic nude mice bearing tumor were evenly and randomly divided into five groups. Each mouse was injected via tail vein with 200 μL free ICG derivative, ICG derivative-loaded SO-chitosan micelles or ICG derivative-loaded folate-SO-chitosan micelles (containing 10 μg ICG derivative). The design of this study was described in detail as follows: (a) each Bel-7402 tumor-bearing mouse was injected with 10 μg free ICG derivative; (b) each Bel-7402 tumor-bearing mouse was injected with ICG derivative-loaded SO-chitosan micelles; (c) each Bel-7402 tumor-bearing mouse was injected intravenously with ICG derivative-loaded folate-SO-chitosan micelles; (d) each A549 tumor-bearing mouse was injected with ICG derivative-loaded folate-SO-chitosan micelles; (e) each Bel-7402 tumor-bearing mouse was injected with ICG derivative-loaded folate-SO-chitosan micelles, with prior injection of free folic acid (2 μmol) for competition assay.

The dynamic behavior of folate-SO-chitosan was monitored by the self-built NIR imaging system, which was introduced in details in our previous work (Chen et al., 2008; Zhang, Chen, Xu, & Gu, 2008). The subjected mouse was firstly anesthetized and imaged at predetermined intervals (0 min, 5 min, 1 h, 6 h, 12 h, 24 h, 48 h and 72 h) post-injection. All fluorescence images were acquired with 1-s exposure (f/stop = 4).

To confirm the *in vivo* distribution of folate-SO-chitosan or SO-chitosan micelles, mice were sacrificed 24 h post-injection. The excised organs and tissues (heart, liver, spleen, lung, kidney and tumor) were also non-invasively imaged by the self-built NIR imaging system.

To quantitatively measure the targeting ability of folate-SO-chitosan, the tumor to background ratio (TBR) was calculated with definition as: TBR = (tumor signal − background signal)/background signal. The NIR fluorescence signal per selected region (5 mm^2) was measured based on the analysis of region of interest (ROI, tumor or normal tissue) from the obtained NIR fluorescence images. The tissue distribution of folate-SO-chitosan or SO-chitosan micelles in excised tissues was also quantified by the same protocol.

2.10. Statistical analysis

To find out the difference between two independent samples, *t*-test was used using SPSS (Version 11.5, SPSS Inc., USA). The means were judged to be different when $P < 0.05$ and significantly different when $P < 0.01$.

3. Results and discussion

3.1. Synthesis and identification of folate-SO-chitosan

As described in the method section (Fig. 1), the long chain alkyl groups served as hydrophobic moieties and succinyl groups served as hydrophilic moieties were respectively reacted to the amino groups in chitosan to form SO-chitosan. Then the SO-chitosan was modified with folate by amide bond.

The UV spectra of chitosan, SO-chitosan, folate and folate-SO-chitosan (Fig. 2A) show that folate-SO-chitosan had both the end absorption of chitosan and the characteristic absorption peaks of folate (280 and 362 nm), which confirmed the folate modification of SO-chitosan.

The FTIR spectrum of SO-chitosan shows a new peak at 1563 cm^{-1} relative to chitosan spectrum (Fig. 2B). This peak is usually caused by secondary amines, suggesting some of the amino groups of chitosan were substituted (Aoki, Nishikawa, & Hattori, 2003). The absorption band at 1729 cm^{-1}, the specific peak of carbonyl groups, testified to the presence of the succinyl group ($-NHCOCH_2CH_2COOH$). The new peaks at 2927 and 2857 cm^{-1}, were attributed to methyl groups due to the long alkyl chain ($-NH-CH_2-(CH_2)_6-CH_3$) and indicated the reaction of octaldehyde to chitosan (Xu et al., 2007). Comparing the FTIR spectra of folate with that of folate-SO-chitosan, the appearance of the peak at 1607 cm^{-1} in the spectrum of folate-SO-chitosan was attributed to benzene ring of the folate.

Comparing the ^1H NMR spectra of chitosan in D_2O and DCl and SO-chitosan in D_2O (Fig. 2C), the new signals at (1.28, 1.52) ppm and 0.86 ppm were assigned to the methene hydrogen and methyl hydrogen of *N*-alkyl group ($-NH-CH_2-(CH_2)_6-CH_3$), respectively. And the new signals at the range of 2.04–2.53 ppm belonged to the methene hydrogen of the succinyl group ($-COCH_2CH_2COOH$). In contrast to the ^1H NMR spectra of SO-chitosan, the further resonance signals at 4.39, 6.89, and 7.71 ppm were found in the ^1H NMR spectra of folate-SO-chitosan in D_2O, which confirmed the existence of folate residues.

From the results of UV, FTIR, and ^1H NMR spectra, we concluded that a part of the amino groups of chitosan were substituted by octyl, succinyl groups and folate, respectively.

3.2. Size and morphology of folate-SO-chitosan micelles

Fig. 3A and B show that the average diameters for folate-SO-chitosan and SO-chitosan micelles were about 136 nm (135.69 ± 28.86 nm, mean ± *SD*, similarly hereinafter) and 199 nm (199.41 ± 22.92 nm), respectively. The stability of the folate-SO-chitosan was also investigated in our research. The mean diameters of folate-SO-chitosan micelles in PBS (pH 7.4) determined at 0, 1, 3, 5, 7 and 15 days post-synthesis were about 137, 142, 144, 149, 150 and 150 nm, respectively (Fig. 3C), which suggested that the micelle

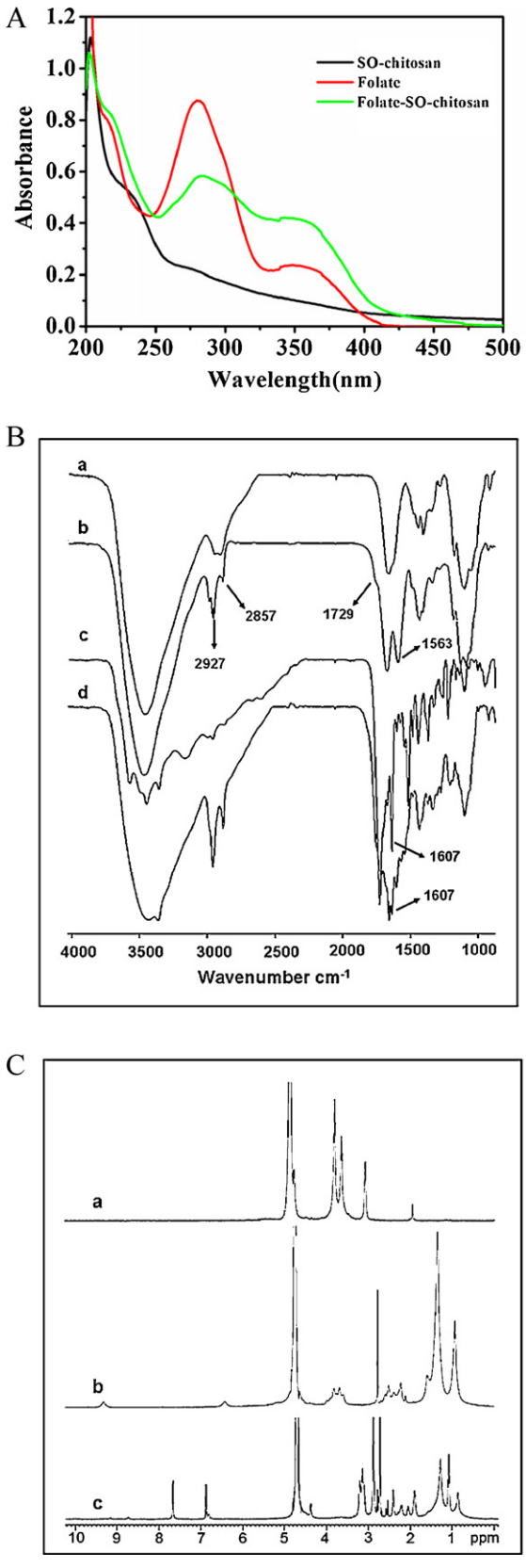

Fig. 2. Identification of SO-chitosan and folate-SO-chitosan with UV, FT-IR and ^{1}H NMR: (A) absorbance of SO-chitosan, folate and folate-SO-chitosan; (B) the FT-IR spectra of (a) chitosan, (b) SO-chitosan, (c) folate and (d) folate-SO-chitosan; (C) the ^{1}H NMR spectra of (a) chitosan in D_2O and DCl, (b) SO-chitosan in D_2O, and (c) folate-SO-chitosan in D_2O.

nanoparticles had satisfactory stability in simulated physiological condition.

From TEM images (Fig. 3D), the average sizes of folate-SO-chitosan and SO-chitosan micelles were both about 90 nm (TEM image of SO-chitosan micelles not shown here). The self-assembled micelles were well dispersed as individual nanoparticles with a near-spherical shape.

Diameters of chitosan-based nanoparticles were determined by several parameters: the content of hydrophobic groups (octyl), the hydration of nanoparticles and the charge density of the main chain. After hydrophobic substitution, a core-shell spherical structure of chitosan-based nanoparticle was established because of the hydrophobic association of octyl groups. This kind of core-shell structure was further strengthened and tightened after hydrophilic substitution with succinyl groups. Thus, the SO-chitosan micelle formed through self-assembling. Without the hydrophobic/hydrophilic substitution, the chitosan macromolecules would be form a long line because of the positive charge caused by amine groups, which would make the solution very sticky. One succinic anhydride molecule could consume one "$-NH_2$" and create a "$-COO^-$", and the newborn "$-COO^-$" could further neutralize the positive charge of another "$-NH_2$". The decrease of the positive charges on the polymer backbone could decrease the tensile force in the backbone of chitosan and reduce the diameter of the micelles. Because of the similar consumption of amine groups by folate, folate-SO-chitosan micelles had smaller diameter (135 nm) compared with that of SO-chitosan micelles (200 nm). So it was speculated that the surface charge does affect the particle size. In addition, the sizes of chitosan micelles measured by LPSA were larger than those observed by TEM. This might be caused by the evaporation of water during the sample preparation of TEM. The dehydration process likely resulted in the shrinkage of the particles (Giacomelli, Schmidt, & Borsali, 2007; Morita, Horikiri, Suzuki, & Yoshino, 2001).

3.3. Drug loading and in vitro drug release of folate-SO-chitosan micelles

Two hydrophobic compounds, fluorescein and ICG derivative, were chosen as model drugs on account of their different solubilities in aqueous solution. The excitation and emission wavelengths for the fluorescein and ICG derivative are 488/525 and 760/808 nm, respectively. The fluorescence ranges of these two model drugs make them suitable for *in vitro* cellular study under microscopy (fluorescein) and *in vivo* targeting evaluation under optical imaging system (ICG derivative), respectively.

When the weight ratio of model drugs and folate-SO-chitosan was 1:5, folate-SO-chitosan had optimal drug loading content of $12.17 \pm 0.63\%$ for fluorescein, but it had drug loading content of just $6.33 \pm 0.54\%$ for ICG derivative. This micellar system also had better entrapment efficiency for fluoresein ($69.32 \pm 3.32\%$) than that for ICG derivative ($33.79 \pm 3.06\%$). Theoretically, the binding force of a drug is the determining factor for the drug loading content and entrapment efficiency within a micelle and is directly related to the drug's hydrophobicity. However, the drug loading content and entrapment efficiency for ICG derivative were less than that of the less hydrophobic fluorescein. This phenomenon could be explained through the drug loading process. In fact, drug loading for the micelles is a dynamic process of drug from the outer medium entering the inner hydrophobic core. The ICG derivative with poor solubility may have precipitated during the dropwise addition into the aqueous phase of chitosan micelles. Precipitation would then result in lower entrapment into the core of folate-SO-chitosan micelles. As a result, lower drug loading content and entrapment efficiency were realized for ICG derivative as a result the drug loading process for folate-SO-chitosan micelles.

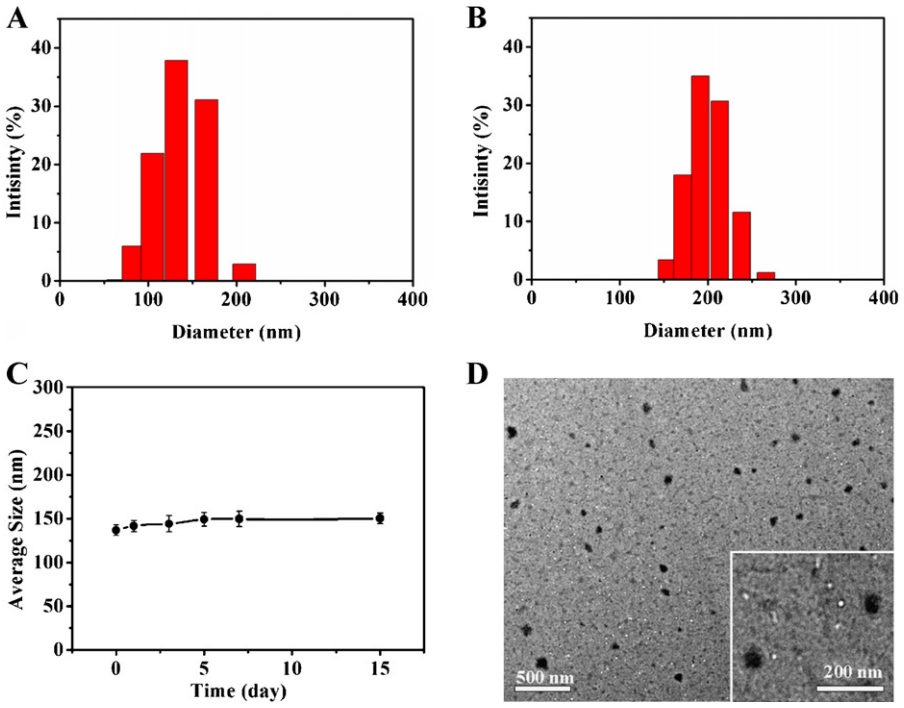

Fig. 3. Size distribution of (A) folate-SO-chitosan and (B) SO-chitosan micelles at 25 °C in PBS (pH 7.4); (C) particle size of folate-SO-chitosan micelles at 25 °C in PBS (pH 7.4) as a function of time; (D) transmission electron microscope (TEM) picture of folate-SO-chitosan micelles.

The *in vitro* release profiles of fluorescein and ICG derivative from micelle nanoparticles are exhibited in Fig. 4A. An apparent initial burst release was observed in the release profile of fluorescein. About 65% of fluorescein was released within the first 10 h. After the initial burst release, the drug release profiles switched to a slow release phase. More than 90% of the loaded fluorescein released from micelle nanoparticles at 75 h post-dialysis. However, ICG derivative loaded folate-SO-chitosan system had nearly no initial burst release and it had a much lower release speed. The cumulative release rates of ICG derivative from micelle nanoparticles at 10 and 75 h were just 7 and 26%, respectively.

These results showed that the release rate of model drugs decreased with the decrease of drug solubility. That is, the release rate of fluorescein was higher than that of ICG derivative. This result

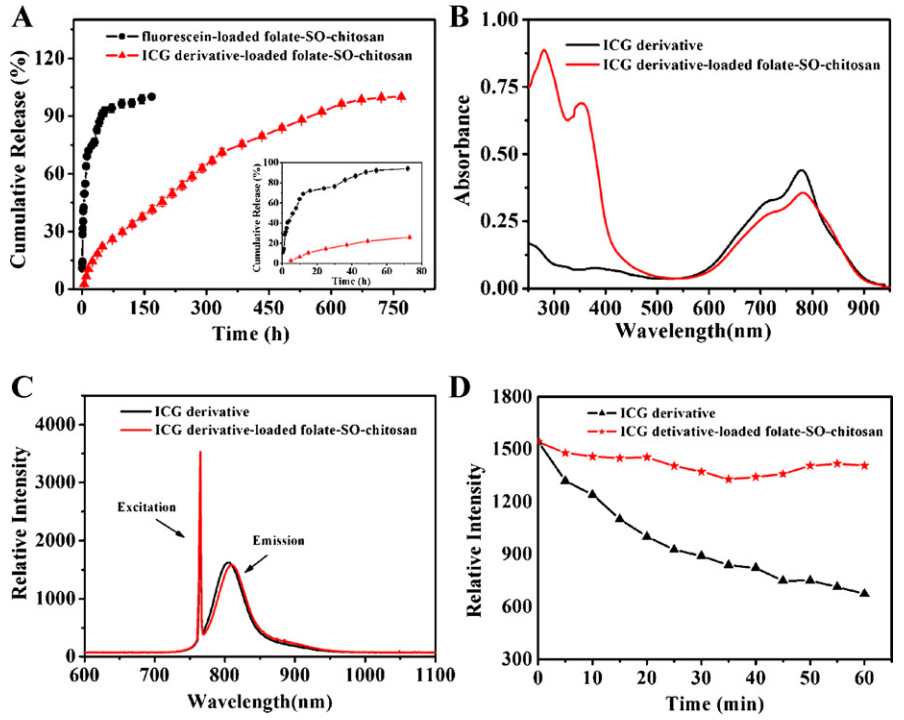

Fig. 4. (A) Release kinetics of fluorescein-loaded folate-SO-chitosan micelles and ICG derivative-loaded folate-SO-chitosan micelles in PBS (pH 7.4, 37 °C). Inset: The release kinetics of the initial 75 h. Data were given as mean ± *SD* (*n* = 3). Optical characterization of free ICG derivative and ICG derivative-loaded folate-SO-chitosan: (B) absorbance spectra; (C) fluorescence spectra; (D) photo stability.

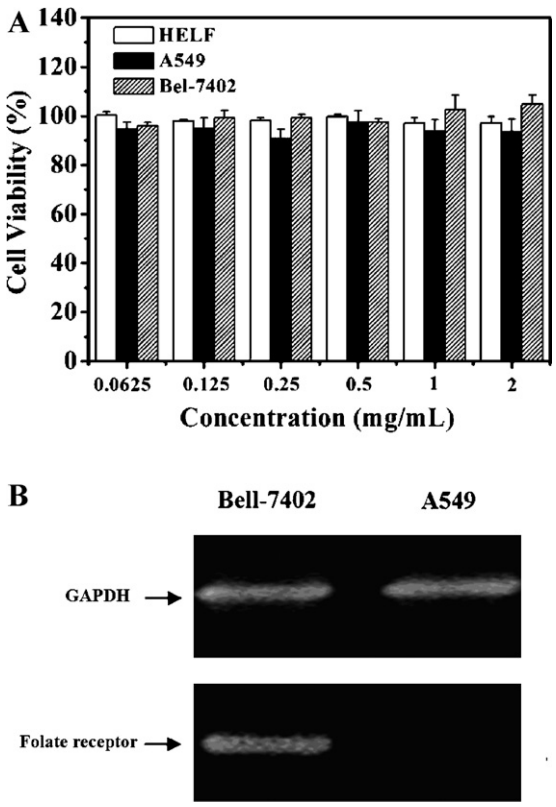

Fig. 5. (A) Cytotoxicity study of folate-SO-chitosan in HELF cells, A549 cells, and Bel-7402 cells. Data represent mean ± *SD* ($n = 5$). (B) Folate receptor expression levels of A549 cells and Bel-7402 cells by Reverse Transcriptase PCR.

is consistent with a similar report by another group (Seidenberger, Siepmann, Bley, Maeder, & Siepmann, 2011).

In addition, the binding force of ICG derivative to micelle is stronger than that of fluorescein because of its higher hydrophobicity, which also induced a lower release rate for ICG derivative from folate-SO-chitosan carrier than that of fluorescein.

3.4. Optical characterization of entrapped ICG derivative

ICG derivative is a hydrophobic dye with absorbance peak at 783 nm and maximum emission at 808 nm. It could be easily entrapped into folate-SO-chitosan by hydrophobic association effect. The spectra of absorption and emission for ICG derivative and ICG derivative loaded folate-SO-chitosan are depicted in Fig. 4B and C. The optical properties of ICG derivative did not change much after the entrapment. However, ICG derivative had much better photostability after being entrapped by folate-SO-chitosan (Fig. 4D). The satisfactory photostability of entrapped ICG derivative made it more suitable to trace the dynamic process of folate-SO-chitosan in the mouse model evaluated by optical imaging.

3.5. Cytotoxicity assay of folate-SO-chitosan micelles

MTT assay was performed to investigate the cytotoxicity of folate-SO-chitosan micelles. The effects of the micelles concentration on the proliferation of HELF, A549 and Bel-7402 were studied (Fig. 5A). Results demonstrated that there were no significant decreases in cell viability even at a concentration of micelles as high as 2 mg/mL. The proof of little or no-cytotoxicity of chitosan-based micelles were also reported elsewhere (Cao et al., 2007).

3.6. In vitro cellular uptake of folate-SO-chitosan micelles

To study the correlation of cell uptake of folate-SO-chitosan micelles with the folate receptor expression, the folate receptor expression levels in tumor cell lines Bel-7402 cells and A549 were assayed by PCR, as showed in Fig. 5B. High folate receptor expression was always displayed in Bel-7402 cells, while there was nearly no folate receptor expression in A549 cells.

In vitro cellular uptake of micelles was evaluated by fluorescence microscopy (Fig. 6A). Fluorescence images of groups a and b (Fig. 6A) show that neither SO-chitosan nor folate-SO-chitosan could enter A549 cells because of the low expression of folate receptor on their surface. In contrast, remarkable fluorescence was observed in Bel-7402 cells incubated with fluorescein-loaded folate-SO-chitosan micelles (Fig. 6A, group d), whereas nearly no fluorescence was observed in that for fluorescein-loaded SO-chitosan (Fig. 6A, group c). The results were attributed to the different folate receptor expression levels of A549 cells and Bel-7402 cells, which indicated that the internalization of folate-SO-chitosan into Bel-7402 is folate receptor-mediated. A competition study of free folic acid with folate-SO-chitosan micelles for Bel-7402 cells was also carried out to better understand the mechanism folate receptor-mediated endocytosis. Because of the competitive binding of folic acid to folate receptor, the endocytosis of Bel-7402 cells for folate-SO-chitosan micelles was distinctly blocked, and thus, much weaker fluorescence (compared to group d) was observed in group e (Fig. 6A).

To quantify the results of folate receptor mediated endocytosis, the flow cytometric analysis was also applied to investigate the cellular uptake behaviors of tumor cells (A549 and Bel-7402) for micelles (SO-chitosan and folate-SO-chitosan). The results acquired by flow cytometer had satisfactory correspondence with that acquired by florescence microscopy (Fig. 6A–C). The results showed that there was no significant difference for the uptake of SO-chitosan and folate-SO-chitosan by A549 cells (Fig. 6C). With the help of folate receptor, Bel-7402 cells could uptake much more folate-SO-chitosan than SO-chitosan (nearly 10-fold, $P < 0.001$, Fig. 6C). And the endocytosis of folate-SO-chitosan was decreased by more than 45% because of the competitive binding of free folic acid to folate receptor (Fig. 6C, $P < 0.05$).

All the results testified that the internalization of folate-SO-chitosan into folate receptor positive tumor cells (Bel-7402) is a kind of folate receptor mediated endocytosis, which could be effectively and competitively blocked by free folic acid.

3.7. In vivo distribution and tumor targeting of folate-SO-chitosan micelles

Fig. 7 shows the *in vivo* dynamic processes of ICG derivative loaded folate-SO-chitosan and corresponding control samples in tumor bearing (Bel-7402 or A549) athymic nude mice evaluated by self-built NIR fluorescence imaging system. Images of group a (Fig. 7A, the control group) show that free ICG derivative had slightly targeting ability toward Bel-7402 tumor tissue. And images of group b (another control group) indicated that ICG derivative-loaded SO-chitosan micelles had a degree of passive targeting effect for Bel-7402 tumor even without the help of folate. Apparent fluorescent signals could be observed from 24 to 48 h post-injection. This passive targeting behavior of non-folate micelles for Bel-7402 tumor tissues was due to the enhanced permeation and retention effect, which was caused by the leaky property of tumor tissues (Iyer, Khaled, & Fang, 2006).

For group c, ICG derivative-loaded folate-SO-chitosan micelles displayed apparent accumulation in Bel-7402 tumor tissues at just 1 h post-injection. The fluorescence intensity in tumor persistently enhanced and reached a maximum at 24 h post-injection.

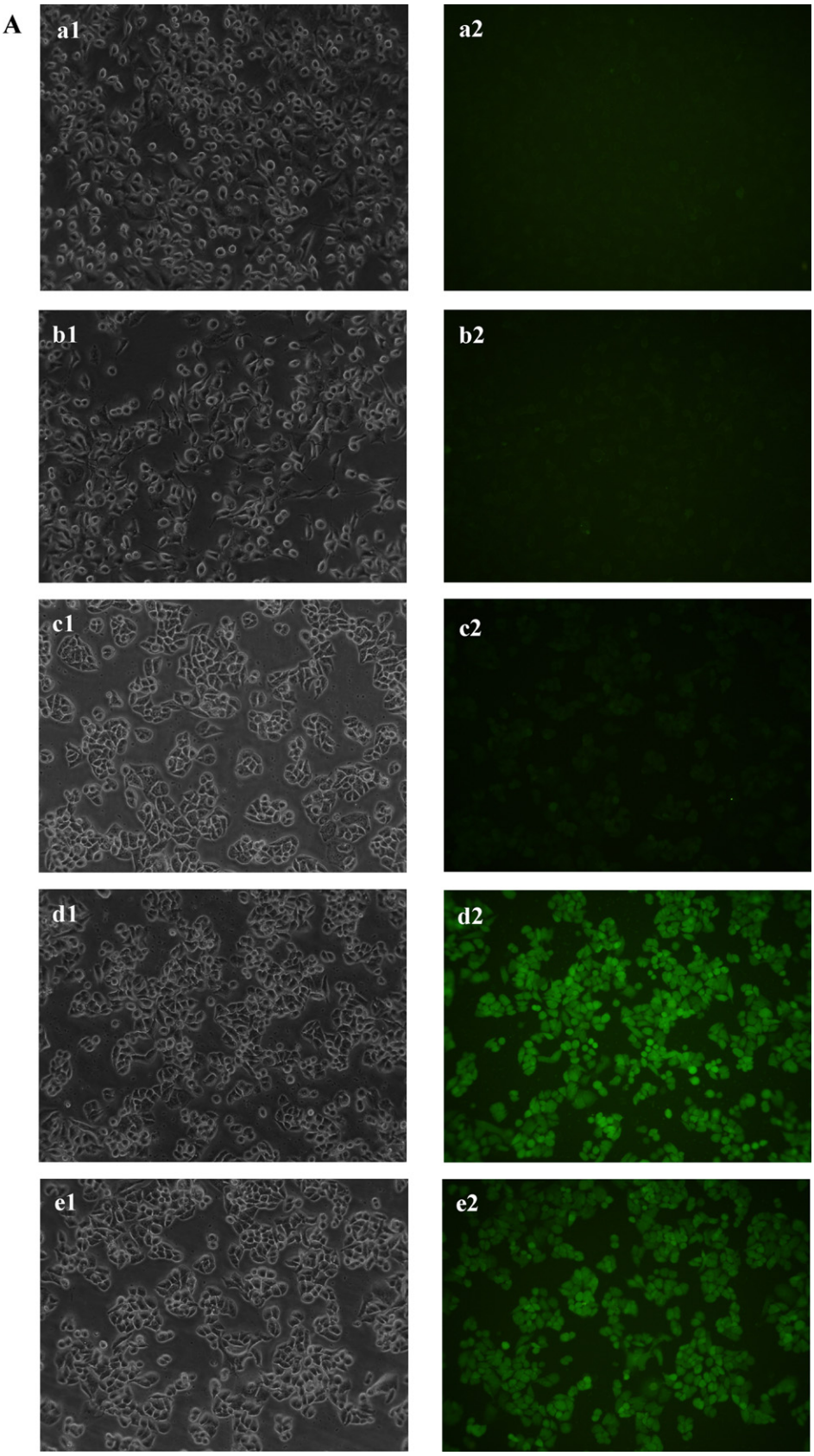

Fig. 6. (A) Microscopy images and (B) flow cytometry histograms of cell uptake: (a) A549 cells incubated with fluorescein-loaded SO-chitosan micelles; (b) A549 cells incubated with fluorescein-loaded folate-SO-chitosan micelles; (c) Bel-7402 cells incubated with fluorescein-loaded SO-chitosan micelles; (d) Bel-7402 cells incubated with fluorescein-loaded folate-SO-chitosan micelles; (e) Bel-7402 cells firstly incubated with free folic acid and then cultured with fluorescein-loaded folate-SO-chitosan micelles for competition assay (a_1, b_1, c_1, d_1, e_1: bright field images; a_2, b_2, c_2, d_2, e_2: fluorescent microscopic images). (C) Mean fluorescence intensity of cells determined by flow cytometry. Data were given as mean ± *SD* ($n = 3$) ($^{**}P < 0.001$, $^{*}P < 0.05$).

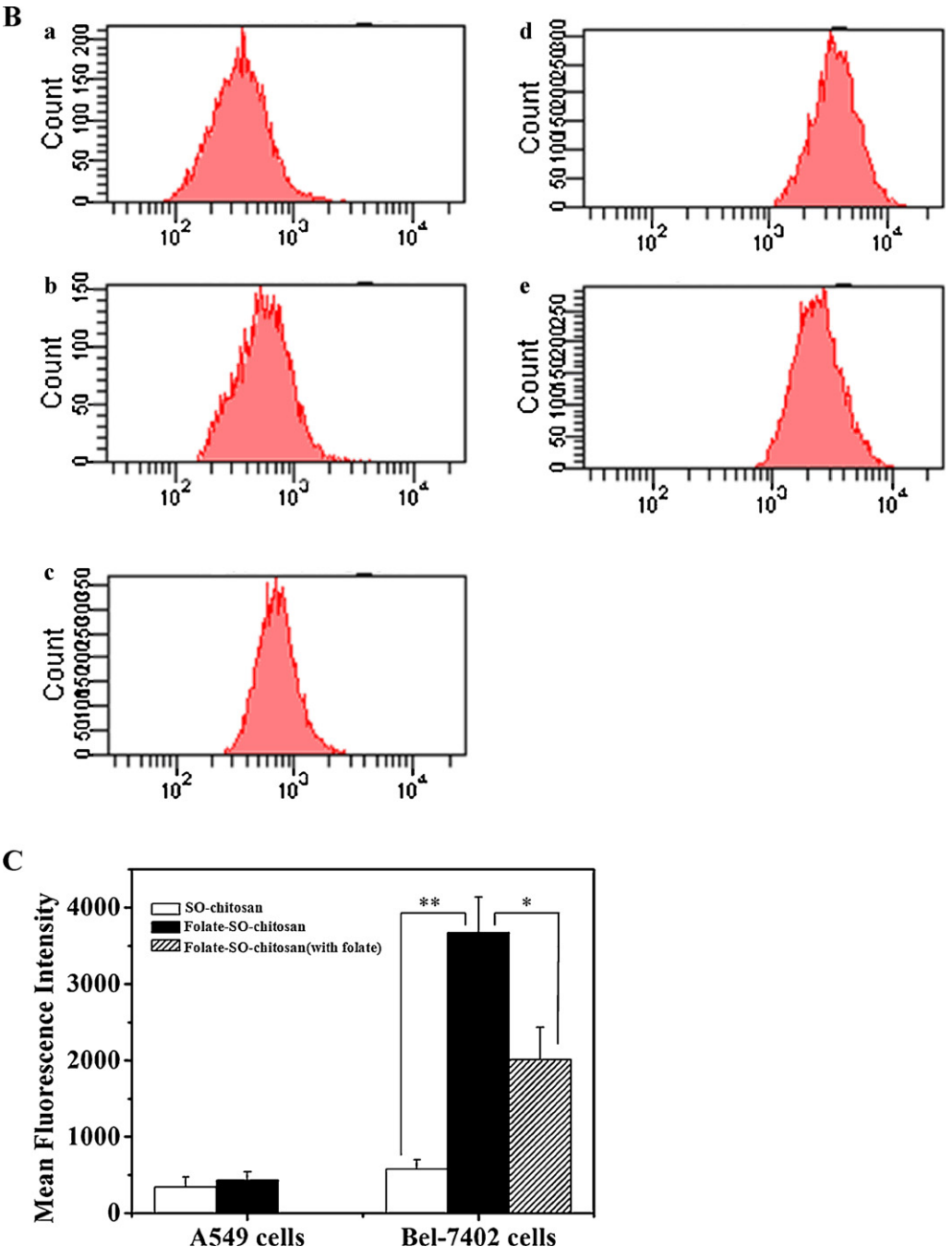

Fig. 6. (*Continued*)

Strong fluorescence could be still observed at 72 h post-injection. Mice in group d were used as a folate receptor negative control test. The images of group d showed that ICG derivative loaded folate-SO-chitosan micelles had a degree of targeting ability for folate receptor negative A549 tumor tissue, just similar to that of non-folate SO-chitosan in the tumor model of Bel-7402. Folate-SO-chitosan showed much better targeting for folate receptor positive tumor model (Bel-7402) than that for folate receptor negative tumor model (A549). In this study, a competitive binding test was also designed and carried out for better understanding the folate receptor mediated tumor targeting mechanism of folate-modified micelles. Because of the competitive binding of free folic acid for folate receptor expressed on the surface of Bel-7402 tumor cells, there was not enough free folate receptor to mediate the endocytosis of folate-SO-chitosan nanoparticles. There was no apparent enhancement of fluorescence signal observed in the tumor site during the first 6 h post-injection (Fig. 7A, group e). With the endocytosis and metabolism of free folic acid, more and more folate receptor could be used for binding folate-SO-chitosan particles. Apparent signals were found in tumor site at 12 h post-injection and the fluorescence intensity kept enhancing and reached the maximum at 24 h post-injection (Fig. 7A). Folate-SO-chitosan had the best targeting capability for folate receptor positive Bel-7402 with TBR up to 16.66 at 24 h post-injection, which was much better than that for folate receptor negative A549 with TBR about 7.09 at 48 h (Fig. 7B). All the results testified that the *in vivo* targeting behavior of this kind of folate-SO-chitosan micelle is folate receptor mediated.

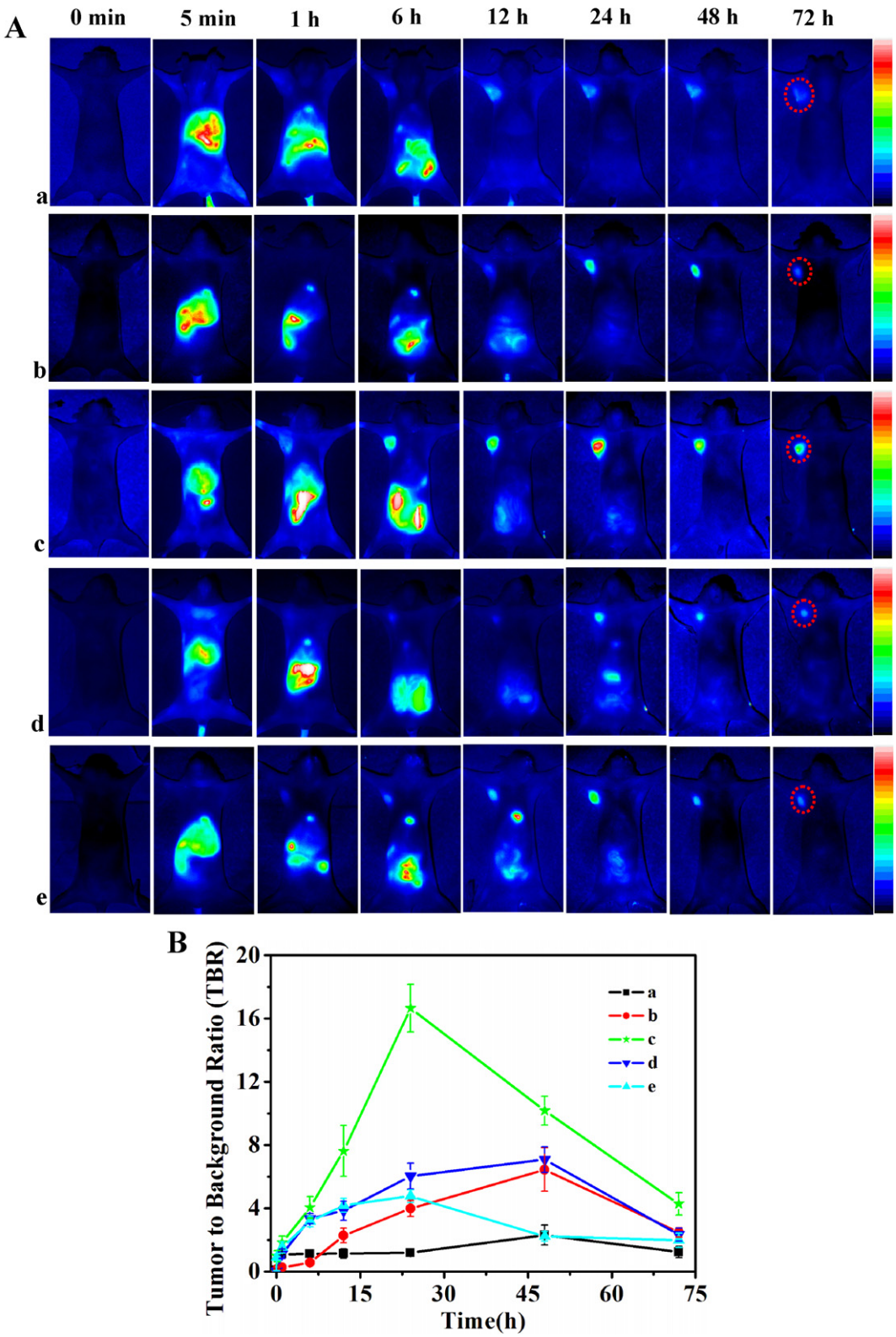

Fig. 7. (A) *In vivo* targeting behavior of folate-SO-chitosan micelles; (B) TBR [tumor to background (muscle) ratio] values: (a) systemic injection of free ICG derivative into Bel-7402 tumor-bearing mice; (b) systemic injection of ICG derivative-loaded SO-chitosan micelles into Bel-7402 tumor-bearing mice; (c) systemic injection of ICG derivative-loaded folate-SO-chitosan micelles into Bel-7402 tumor-bearing mice; (d) systemic injection of ICG derivative-loaded folate-SO-chitosan micelles into A549 tumor-bearing mice; (e) systemic injection of ICG derivative-loaded folate-SO-chitosan micelles into Bel-7402 tumor-bearing mice, with prior injection of free folate (2 μmol) for competition assay. Data were given as mean ± *SD* ($n = 5$).

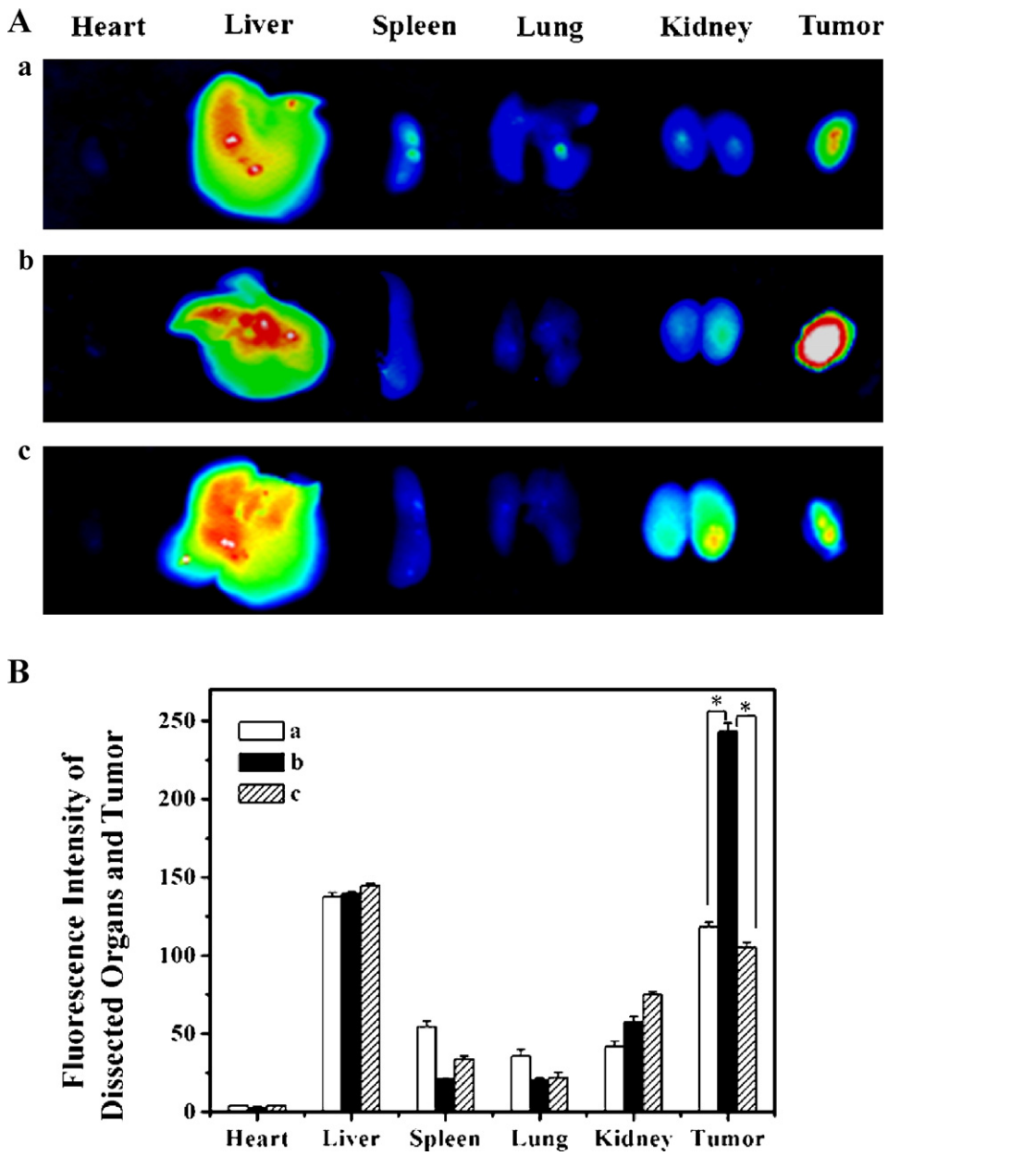

Fig. 8. (A) Representative *ex vivo* NIR fluorescence images and (B) fluorescence intensity of dissected organs and tumors of mice (a and b: Bel-7402 tumor-bearing mice; c: A549 tumor-bearing mice) sacrificed at 24 h, after i.v. injection of micelle nanoparticles (a: ICG derivative-loaded SO-chitosan; b and c: ICG derivative-loaded folate-SO-chitosan). Data were given as mean ± *SD* ($n = 5$) (*$P < 0.001$).

To verify the *in vivo* biodistribution of ICG derivative-loaded folate-SO-chitosan and SO-chitosan micelles monitored by NIR imaging system, mice were sacrificed at 24 h post-injection and *ex vivo* NIR fluorescence images of the excised tissues/organs were conducted. As shown in Fig. 8A and B, folate-SO-chitosan micelles showed significantly higher accumulation for folate receptor positive tumor model (Bel-7402) than those for folate receptor negative tumor model (A549) (243 a.u. for folate-SO-chitosan in Bel-7402 and 105 a.u. for folate-SO-chitosan in A549, $P < 0.001$). Compared with SO-chitosan micelles, folate-SO-chitosan micelles also resulted in much better tumor targeting with the higher fluorescence intensity in the Bel-7402 tumor (243 a.u. for folate-SO-chitosan and 118 a.u. for SO-chitosan in Bel-7402, $P < 0.001$). All these results supplied a decisive evidence of satisfactory tumor targeting capability of folate-SO-chitosan micelles.

Previously, the Xu group reported doxorubicin-loaded SO-chitosan micelles with effective anti-tumor activity (Xu et al., 2007). Here we report folate-modified SO-chitosan micelles for enhanced tumor-specific delivery and demonstrate *in vivo* tumor targeting capability and dynamic distribution of SO-chitosan micelles in animals. Generally, the tumor targeting ability of nanoparticles may be enhanced through enhanced permeation and retention effect. In order to further improve the tumor targeting ability, folate-modified SO-chitosan micelles were prepared in this study. It was shown that the cellular uptake and unique accumulation behavior in folate receptor positive tumors were significantly enhanced after the modification of SO-chitosan micells with the active ligand, folate. This enhancement indicated that the tumor targeting ability of folate-SO-chitosan micelles is mainly mediated by folate receptor. In addition, because of the excellent tumor targeting capability and the satisfactory biocompatibility of the folate-SO-

chitosan micelles, other diagnostic agents could be loaded and serve in the early tumor diagnosis for folate receptor positive tumors by different imaging modalities, such as the commonly used magnetic resonance imaging (MRI) and NIR optical imaging.

4. Conclusions

Folate-modified N-succinyl-N′-octyl chitosan micelles were synthesized in this study and maintained stable structure up to 15 days with average diameter of 136 nm. Drug loading and release results indicated that the folate-SO-chitosan micelles had the satisfactory drug loading content, entrapment efficiency and sustained release behavior for model drugs, in this case, fluorescent reporter dyes. The tumor targeting effect of the folate-SO-chitosan micelles was clearly demonstrated by NIR imaging system in folate receptor-positive Bel-7402 tumor tissue, which indicated the potential application of folate-SO-chitosan micelles in the targeted diagnosis and therapy to different kinds of folate receptor positive tumors. The tumor targeting of anti-tumor therapy loaded in this delivery system requires further research.

Acknowledgments

This research was supported by the Natural Science Foundation Committee of China (NSFC refid=ğs0005ȳ30672015, 30700779, 30800257, 30970776, 81000666, 81071194, 31050110123) and the major project from the Ministry of Science and Technology for new drug development (2009ZX09310-004).

References

Aoki, N., Nishikawa, M., & Hattori, K. (2003). Synthesis of chitosan derivatives bearing cyclodextrin and adsorption of *p*-nonylphenol and bisphenol A. *Carbohydrate Polymers*, *52*, 219–223.

Calvo, P., Remunan, C., Vila, J. L., & Alonso, M. J. (1997). Chitosan and chitosan ethylene oxide propylene oxide block copolymer nanoparticles as novel carriers for proteins and vaccines. *Pharmaceutical Research*, *14*, 1431–1436.

Cao, Y. X., Zhang, C., Shen, W. B., Cheng, Z. H., Yu, L. L., & Ping, Q. N. (2007). Poly(N-isopropylacrylamide)–chitosan as thermosensitive in situ gel-forming system for ocular drug delivery. *Journal of Controlled Release*, *120*, 186–194.

Chen, H. Y., Zhang, J., Qian, Z. Y., Liu, F., Chen, X. Y., & Gu, Y. Q. (2008). In vivo non-invasive optical imaging of temperature-sensitive co-polymeric nanohydrogel. *Nanotechnology*, *19*, 185707–185716.

Corot, C., Robert, P., Lancelot, E., Prigent, P., Ballet, S., Guilbert, I., et al. (2008). Tumor imaging using P866, a high-relaxivity gadoliniumchelate designed for folate receptor targeting. *Magnetic Resonance in Medicine*, *60*, 1337–1346.

Felt, O., Buri, P., & Gurny, R. (1998). Chitosan: A unique polysaccharide for drug delivery. *Drug Development and Industrial Pharmacy*, *24*, 979–993.

Gan, C. W., & Feng, S. S. (2010). Transferrin-conjugated nanoparticles of poly(lactide)-D-α-tocopheryl polyethylene glycol succinate diblock copolymer for targeted drug delivery across the blood–brain barrier. *Biomaterials*, *31*, 7748–7757.

Giacomelli, C., Schmidt, V., & Borsali, R. (2007). Nanocontainers formed by self-assembly of poly(ethylene oxide)-b-poly(glycerol monomethacrylate)-drug conjugates. *Macromolecules*, *40*, 2148–2157.

Hilgenbrink, A. R., & Low, P. S. (2005). Folate receptor-mediated drug targeting: From therapeutics to diagnostics. *Journal of Pharmaceutical Sciences*, *94*, 2135–2146.

Hirano, S., Zhang, M., Nakagawa, M., & Miyata, T. (2000). Wet spun chitosan-collagen fibers, their chemical N-modifications, blood compatibility. *Biomaterials*, *21*, 997–1003.

Hu, F. Q., Zhao, M. D., & Yuan, H. (2006). A novel chitosan oligosaccharideestearic acid micelles for gene delivery: Properties and in vitro transfection studies. *International Journal of Pharmaceutics*, *315*, 158–166.

Illum, L. (1998). Chitosan and its use as a pharmaceutical excipient. *Pharmaceutical Research*, *15*, 1326–1331.

Iyer, A. K., Khaled, G., & Fang, J. (2006). Exploiting the enhanced permeability and retention effect for tumor imaging. *Drug Discovery Today*, *11*, 812–818.

Kamaly, N., Kalber, T., Thanou, M., Bell, D. B., & Miller, A. D. (2009). Folate receptor targeted biomodal liposomes for tumor magnetic resonance imaging. *Bioconjugate Chemistry*, *20*, 648–655.

Leamon, C. P., & Low, P. S. (2001). Folate-mediated targeting: From diagnostics to drug and gene delivery. *Drug Discovery Today*, *6*, 44–51.

Maeda, H., Bharate, G. Y., & Daruwalla, J. (2009). Polymeric drugs for efficient tumor-targeted drug delivery based on EPR-effect. *European Journal of Pharmaceutics and Biopharmaceutics*, *71*, 409–419.

Mi, F. L., Shyu, S. S., Kuan, C. Y., Lee, S. T., Lu, K. T., & Jang, S. F. (1999). Chitosan-polyelectrolyte complexation for the preparation of gel beads and controlled release of anticancer drug. I. Effect of phosphorous polyelectrolyte complex and enzymatic hydrolysis of polymer. *Journal of Applied Polymer Science*, *74*, 1868–1879.

Morita, T., Horikiri, Y., Suzuki, T., & Yoshino, H. (2001). Preparation of gelatin microparticles by co-lyophilization with poly(ethylene glycol): Characterization and application to entrapment into biodegradable microspheres. *International Journal of Pharmaceutics*, *219*, 127–137.

Park, J. H., Kwon, S., Nam, J. O., Park, R. W., Chung, H., Seo, S. B., et al. (2004). Self-assembled nanoparticles based on glycol chitosan bearing 5beta-cholanic acid for RGD peptide delivery. *Journal of Controlled Release*, *95*, 579–588.

Rege, P. R., Garmise, R. J., & Block, L. H. (2003). Spray-dried chitinosans. Part II. In vitro drug release from tablets made from spray-dried chitinosans. *International Journal of Pharmaceutics*, *252*, 53–59.

Rege, P. R., Shukla, D. J., & Block, L. H. (1999). Chitinosans as tableting excipients for modified release delivery systems. *International Journal of Pharmaceutics*, *181*, 49–60.

Rösler, A., Vandermeulen, G., & Klok, H. (2001). Advanced drug delivery devices via self-assembly of amphiphilic block copolymers. *Advanced Drug Delivery Reviews*, *53*, 95–108.

Saad, M., Garbuzenko, O. B., Ber, E., Chandna, P., Khandare, J. J., Pozharov, V. P., et al. (2008). Receptor targeted polymers, dendrimers, liposomes: Which nanocarrier is the most efficient for tumor-specific treatment and imaging? *Journal of Controlled Release*, *130*, 107–114.

Sabharanjak, S., & Mayor, S. (2004). Folate receptor endocytosis and trafficking. *Advanced Drug Delivery Reviews*, *56*, 1099–1109.

Seidenberger, T., Siepmann, J., Bley, H., Maeder, K., & Siepmann, F. (2011). Simultaneous controlled vitamin release from multiparticulates: Theory and experiment. *International Journal of Pharmaceutics*, *412*, 68–76.

Tomihata, K., & Ikada, Y. (1997). In vitro and in vivo degradation of films of chitin and its deacetylated derivatives. *Biomaterials*, *18*, 567–575.

Wei, H., Cheng, S., Zhang, X., & Zhuo, R. (2009). Thermo-sensitive polymeric micelles based on poly(N-isopropylacrylamide) as drug carriers. *Progress in Polymer Science*, *34*, 893–910.

Xu, X. Y., Li, L., Zhou, J. P., Lu, S. Y., Yang, J., Yin, X. J., et al. (2007). Preparation and characterization of N-succinyl-N′-octyl chitosan micelles as doxorubicin carriers for effective anti-tumor activity. *Colloids and Surfaces B: Biointerfaces*, *55*, 222–228.

Zhang, J., Chen, H. Y., Xu, L., & Gu, Y. Q. (2008). The targeted behavior of thermally responsive nanohydrogel evaluated by NIR system in mouse model. *Journal of Controlled Release*, *131*, 34–40.

Zhang, C., Ding, Y., Yu, L. L., & Ping, Q. N. (2007). Polymeric micelle systems of hydroxycamptothecin based on amphiphilic N-alkyl-N-trimethyl chitosan derivatives. *Colloids and Surfaces B: Biointerfaces*, *55*, 192–199.